Materials Science and Engineering, B12 (1992) 307–325

The role of extended defects on transient boron diffusion in ion-implanted silicon

R. J. Schreutelkamp*, J. S. Custer, V. Raineri†, W. X. Lu‡, J. R. Liefting and F. W. Saris
FOM Institute for Atomic and Molecular Physics, Kruislaan 407, 1098 SJ Amsterdam (Netherlands)

K. T. F. Janssen
Philips Research Laboratories, P.O. Box 80.000, 5600 JA Eindhoven (Netherlands)

P. F. H. M. van der Meulen and R. E. Kaim
Varian Implant Systems, Blackburn Industrial Park, Dory Road, Gloucester, MA 01930-2297 (USA)

(Received April 18, 1991)

Abstract

Transient tail diffusion of boron in Si(100) has been investigated as a function of boron implant condition, dose, energy, time, temperature and silicon or germanium post-implantations at doses above and below the amorphization threshold. Boron was implanted at energies in the range 5–380 keV and at doses in the range 2×10^{12} to 5×10^{15} cm^{-2} either along [100] or in a random direction. Significantly longer transient boron tail diffusion is observed for implants along [100]. These results reflect the differences between the random and channeling implants in the position of the damage distribution relative to the boron profile. Post-implantation with 1 MeV ^{29}Si ions below the amorphization threshold can reduce boron tail diffusion if the silicon dose is high enough (5×10^{13} cm^{-2} or greater) to form extended defects during the anneal. Lower silicon doses do not influence boron diffusion. Annealing of extended defects also results in anomalous diffusion. These results demonstrate that silicon interstitials cause the enhanced boron diffusion. Amorphization of boron-implanted silicon with ^{29}Si or ^{73}Ge ions prevents transient boron tail diffusion during subsequent annealing if the boron profile is completely incorporated in the amorphized region.

1. Introduction

Very large scale integration (VLSI) of semiconductor devices demands shallow (approximately 0.1 μm) pn junctions [1, 2]. The use of boron implantation in crystalline silicon (c-Si) to form the junctions is limited by two main effects. Firstly, low-energy boron ions in c-Si have a high probability for channeling [3], resulting in deep channeling tails [4] even for "randomly" oriented wafers. The channeling effect of low-energy boron ions can be prevented by pre-amorphization with silicon [5, 6], germanium [7—10] or arsenic [11] ions. However, channeling can be advantageous because of steep profiles. The use of channeling implants seems in contradiction with the demand for shallow (approximately 0.1 μm) pn junctions in VLSI silicon devices. However, Bader and Kalbitzer [12] showed in the early days of ion implantation that channeling boron implants at low energy (6 keV) can be used to produce shallow pn junctions.

The second effect which limits the formation of shallow pn junctions is that boron ions exhibit anomalous diffusion during the high-temperature treatment required to anneal out the implant damage and to activate the dopants. A large number of investigations have concentrated on the anomalous boron tail diffusion (*i.e.* diffusion which is significantly larger than the intrinsic boron diffusion) in silicon during high-temperature annealing and several review papers have been published [6, 13, 14]. The anomalous tail diffusion is transient in nature; significant motion of boron atoms at low concentrations stops within 10 s during annealing at temperatures of 900 °C or higher. Similar anomalous diffusion behavior has also been observed for other dopant species such as phosphorus [15–19].

One way to avoid anomalous boron tail diffusion is by pre-amorphization. However, recrystallization of the amorphized layer and subsequent high-temperature treatment to activate the dopants lead to so-called "end of range" (EOR) defects [20, 21] which deterior-

*Present address: IMEC vzw, Kapeldreef 75, B-3001 Heverlee, Belgium.

†Permanent address: Universita di Catania, Dipartimento di Fisica, 57 Corso Italia, I 95129 Catania, Italy.

‡Permanent address: Institute of Low Energy Nuclear Physics, Beijing Normal University, Beijing 100875, China.

0921-5107/92/$5.00

ate the quality of a pn junction. Ajmera and Rozgonyi [22] solved this issue for silicon- and germanium-pre-amorphized silicon by optimizing the implant and annealing parameters to minimize the interstitial point defect concentration in the EOR region and to stimulate the role of the free surface for annihilation of point defects by control of the ambient. Another way to avoid transient boron diffusion is by post-amorphization with silicon or germanium ions [6, 23, 24]. The formation of EOR defects is also a problem with this method. The advantage over pre-amorphization, however, is that sharp junctions can be obtained using channeled implants [23, 25], whereas the boron profile in pre-amorphized silicon is always gaussian.

Despite many investigations there is still no consensus on the mechanism underlying the transient diffusion. In one of the first models proposed to explain the phenomenon it was assumed that interstitial boron in the (channeling) tail of the implantation profile diffuses rapidly during high-temperature annealing until interaction with a vacancy occurs and normal intrinsic diffusion sets in [26–29]. Many others [16, 30, 31] have suggested that anomalous boron diffusion is associated with the implant damage. In a similar manner to the first model, any boron interstitials are regarded as fast diffusers, but kick-out of substitutional boron by silicon interstitials leads to further fast diffusion. Here, transient boron diffusion will continue until the silicon interstitial concentration reaches equilibrium. Various experiments have shown the enhancement of dopant diffusion under continuous point defect generation. In early papers, diffusion of boron and phosphorus, enhanced by point defects generated by implants of protons [32] and neutrals [33] was demonstrated in boron- and phosphorus-prediffused silicon. Moreover, oxidation [34] and nitridation [35] experiments have illustrated that injected silicon interstitials enhance boron diffusion. Excess interstitials may also arise from the implant of the dopants. Anomalous diffusion of boron and phosphorus in silicon was demonstrated to occur during implantation if the implants were carried out at elevated temperatures [33]. Mobile point defects in implanted silicon may also arise during annealing by various processes, depending on the degree of damage present [36]. They may result from annealing extended defects [30] or from dissociation of clusters of silicon interstitials which are formed during implantation [6, 37].

Recent work by Metzner *et al.* [38] has shown that, during room temperature implants, only about 20% of boron ions come to rest on substitutional lattice sites. Therefore the model of a fast diffusing interstitial boron atom during annealing is tempting because the majority of boron atoms are available immediately for fast diffusion. However, 80% of the boron atoms are available as interstitials for a random implant and thus a channeling implant can only result in 25% more interstitial boron atoms. This difference is insufficient to explain the discrepancies in tail diffusion found in experiments employing random *vs.* channeling implant conditions. In these experiments, it has been shown that the transient tail diffusion of channeled boron is larger than for the random implants, but the total number of rapidly diffusing boron atoms is largest for random implants [23, 39, 40]. Furthermore, Oehrlein *et al.* [16] argued that the transient boron diffusion cannot be attributed solely to interstitial boron atoms because of their high diffusivity at low temperatures. Michel *et al.* [31] showed that for low-dose boron implants the number of boron atoms participating in the anomalous diffusion process increases with temperature. Based on the model of fast diffusing interstitial boron, we would expect their number to be independent of the anneal temperature.

In an attempt to resolve the issue of anomalous boron diffusion in silicon, Hopkins *et al.* [28] removed the near-surface damage region of boron-implanted silicon by a chemical etch prior to annealing. They found no difference in boron diffusion after annealing relative to an unetched sample. Therefore they concluded that the anomalous boron tail diffusion is not associated with implant damage in the region near the peak of the boron profile. In contrast, a similar experiment by Fan *et al.* [41] showed that transient diffusion is avoided if most of the implant damage is removed by an anodic etch. Therefore they concluded that their results did not support the model excluding implant damage. Furthermore, Michel *et al.* [31] suggested that, in the experiment by Hopkins *et al.* [28], not all of the damage region is removed because defect clusters extend to much larger depths [42] than the boron profile, and thus the experiment did not rule out diffusion enhancement by defects.

Cho *et al.* [36] have shown that transient boron diffusion persists in ^{11}B-ion-implanted and annealed silicon if an additional implant with ^{10}B ions is performed which is followed by a second anneal. After the first anneal, the ^{11}B atoms are on substitutional sites, and therefore they associated the enhanced diffusion during the second anneal with implantation damage and not with rapidly diffusing interstitial boron. However, part of the substitutional ^{11}B atoms may have been displaced during the second implant [31, 43] and thus the result does not necessarily rule out the model based solely on anomalously diffusing interstitial boron.

Kim *et al.* [44, 45] have shown that for low-dose boron implants in silicon (1×10^{14} cm^{-2} at 15 keV) anomalous boron tail diffusion saturates within 10 s at 1000 °C. They attributed this result to the rapid

decrease in the concentration of mobile interstitials during the initial stage of annealing and to the absence of extended defects which may act as a source for interstitials during prolonged annealing. For higher doses they observed that the anomalous diffusion persists after annealing for 10 s and is dependent on the annealing behavior of the extended defects. They associated this continuing anomalous boron diffusion with the (partial) annealing of extended defects. This was also concluded by Bao and coworkers [46, 47] for higher energy boron implants.

Recently, many experiments have concentrated on the effect of an additional implant of silicon ions in boron-implanted silicon on the transient boron diffusion behavior. Silicon implantation leads to a supersaturation of point defects without the introduction of impurities. Thus the influence of (additional) implant damage on boron diffusion can be further studied. Michel *et al.* [48] found in such an experiment that anomalous boron tail diffusion is retarded during furnace annealing at 800 °C if, in addition to 2×10^{14} cm^{-2}, 60 keV boron ions, an implant of 130 keV silicon ions to a dose of 2×10^{14} cm^{-2} or higher is performed. In contrast, Packan and Plummer [49] showed in a similar experiment, but with a lower silicon dose (10^{12}–10^{14} cm^{-2}), that anomalous boron diffusion is enhanced at high temperatures by increasing the dose of the implanted silicon ions. Raineri *et al.* [50] illustrated that anomalous boron tail diffusion in silicon implanted with 1×10^{13} cm^{-2}, 10 keV boron ions along [100] was significantly reduced if 1.0 MeV silicon ions were implanted at a dose of 5×10^{13} cm^{-2} or higher. They showed that the reduction of anomalous boron diffusion is accompanied by the formation of secondary defects at a depth of about 1 μm, the silicon damage peak.

The discussion above demonstrates that it is worthwhile to investigate more extensively the role of (extended) defects in the transient diffusion mechanism. In this paper, we present the experimental details and results on transient diffusion studies after channeling implantation. It is shown that the formation of extended defects within the boron profile has no influence on anomalous boron tail diffusion. The effect of megaelectronvolt silicon irradiation on transient boron diffusion has been studied as a function of silicon dose and it is shown that, in this case, the formation of deep extended defects does affect transient boron tail diffusion. The dissolution of extended defects is shown to result in enhanced boron diffusion. It is demonstrated that transient diffusion can be avoided by amorphization. Our results are compared with a qualitative model on the role of boron kick-out by interstitial silicon and trapping by extended defects.

2. Experimental details

Implantations of ^{11}B ions were performed with a Varian/Extrion 220 medium current ion implanter at Varian/Extrion [51]. Boron implantations were performed in either the [100] direction or in a random direction in 150 mm, 1–20 Ω cm, n-type Czochralski-grown silicon wafers of (100) substrate orientation. Boron beam currents were limited to 100 μA to avoid beam heating effects. All implants were performed at room temperature without intentional wafer cooling. The random direction corresponded to a tilt of 10° off normal and a twist of 15° with respect to the flat positioned horizontally. Boron energies were in the range 5–380 keV with doses between 2×10^{12} and 5×10^{15} cm^{-2}. Samples (1.5 cm × 1.5 cm) were cut out of the silicon wafers for silicon or germanium irradiations, thermal treatments or beam analysis. Implants of ^{28}Si, ^{29}Si or ^{73}Ge ions were performed at the megaelectronvolt ion implantation facility at the FOM [52]. Post-amorphization implants with 100–550 keV ^{28}Si or ^{73}Ge ions were carried out with doses in the range 2×10^{14} to 1×10^{15} cm^{-2} at sample temperatures between −60 and −100 °C. Damage irradiations were performed with 1 MeV ^{29}Si ions at doses of 1×10^{10} to 5×10^{14} cm^{-2} at room temperature.

Implanted samples were annealed in a standard vacuum furnace with a base pressure of less than 10^{-7} Torr, or in an AG Associates 401 or a Sitesa-Addax RM rapid thermal processor. Rapid thermal annealing (RTA) was performed under continuous argon or nitrogen flow.

Implanted and annealed samples were investigated by Rutherford backscattering spectrometry (RBS) with 2.0 MeV helium ions in the [100] channeling direction to determine the implant damage, amorphized layer thickness or the formation of secondary defects. The backscattered helium ions were detected with a standard surface barrier detector ($\delta E \approx 15$ keV at 0 °C) at a backscattering angle θ of 120° or 170°.

Cross-sectional transmission electron microscopy (XTEM) and plan-view TEM were used to study secondary defects. Samples for XTEM were thinned using standard mechanical and ion milling procedures. Observations were made in bright-field mode along [011]. Samples for plan-view analysis were thinned by a chemical etch from the backside in a solution of $3HF–6HNO_3–2CH_3COOH$.

Boron concentration profiles were measured by secondary ion mass spectrometry (SIMS) using a Cameca IMS 3f or 4f. The 5 and 10 keV boron profiles were measured using a primary beam of 3.0 keV, 0.25 μA O_2^+ in an oxygen ambient in order to resolve the near-surface part of the profile ($p(O_2) = 2 \times 10^{-5}$ Torr).

For higher energy boron-implanted samples a primary beam of 6.5 keV, 0.7 μA O_2^+ was used. The scanned area was 250 μm × 250 μm and the diameter of the analyzed area was 60 μm.

3. Results

3.1. Transient boron tail diffusion

Channeled implants are perfectly suited for the formation of a well-defined pn junction because of the sharpness of the transition from the p- to n-doped region. The steep decay of the boron profile for a channeled implant is due to the strong reduction in the (nuclear) energy loss straggling of the channeled ions compared with an implant in a random direction. Figure 1 shows the depth distributions for channeled boron implants at energies in the range 5–380 keV with the profiles normalized to a dose of 1×10^{13} cm^{-2} (actual doses ranged from 2×10^{12} cm^{-2} for the lowest energies to 2×10^{14} cm^{-2} for the highest energy). The sharp decrease in boron concentration at the maximum penetration depth, 23 ± 2 decades μm^{-1}, is nearly independent of implant energy. The depth of maximum penetration R_{max} is defined as the depth required to stop all but 1% of the particles [53]. Excellent agreement is found between our experimentally determined values of R_{max} and the calculated values based on the modified Firsov theory [54], as the differrence between the two values is smaller than 5% for all implants [55].

During thermal annealing to remove the ion implantation damage and to activate the implanted dopants, boron diffusion takes place. The effect of RTA at 900 °C is illustrated in Fig. 2 for a channeled implant of 1×10^{13} cm^{-2}, 10 keV ^{11}B ions. The SIMS ^{11}B profiles are shown after implantation (a) and after anneals for 10 s (b) and 20 s (c) at 900 °C. Anomalous boron diffusion is observed in the tail of the profiles after annealing. The boron diffusion is much larger than for the normal intrinsic mechanism ($L_{intr} \approx 1$ nm for 10 s at 900 °C, where L_{intr} represents the intrinsic diffusion length [56]. The anomalous diffusion stops within 10 s and therefore can be referred to as transient. The boron concentrations do not exceed the intrinsic carrier concentration ($n_i = 6 \times 10^{18}$ cm^{-3} at 900 °C), and thus concentration-enhanced diffusion is negligible [57]. The result illustrates the dramatic effect of annealing on the depth and sharpness of the junction.

The anomalous tail diffusion observed in Fig. 2 is not seen only for channeling implants. This is illustrated in the profiles of Fig. 3 for implants of 1×10^{13} cm^{-2}, 5 keV ^{11}B ions in [100] and random directions. The SIMS profiles are shown for as-implanted samples (a) and after RTA for 10 s at 900 °C (b) and 1100 °C (c). For both implant conditions anomalous transient boron tail diffusion is observed. In the tail region the transient diffusion is larger for the implants along [100] than along a random direction. For example, the depth at which the boron concentration is 1×10^{16} cm^{-3} shifts by 50 nm for the channeling implants and only 25 nm for the random implants. Significant boron displacement is observed in the random implant up to a concentration of approximately 8×10^{17} cm^{-3}, whereas for the channeling implant only boron below a concentration of approximately 6×10^{16} cm^{-3} moves significantly. This suggests that the number of boron atoms showing anomalous diffusion is larger for the random implants than for the channeling implants.

The amount of disorder produced in the boron-implanted silicon depends on the implant conditions. In general, a random implant leads to a larger number of displaced silicon atoms than a channeled implant. The annealing behavior of two particular samples is illustrated in the plan-view transmission electron micrographs shown in Fig. 4. The results are demonstrated for samples implanted with 1×10^{13} cm^{-2}, 5

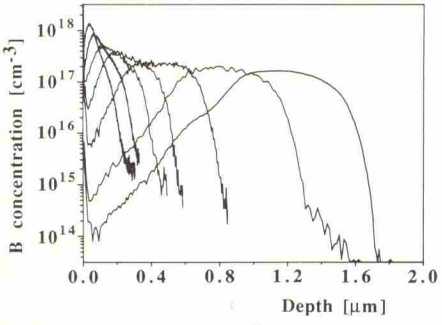

Fig. 1. SIMS profiles of ^{11}B ions implanted in Si(100) showing the energy dependence for channeling implants along [100]. The implants were performed at energies of 5, 10, 20, 40, 80, 200 and 380 keV. All doping profiles were normalized to a dose of 1×10^{13} cm^{-2}. The decay in the boron concentration at R_{max} is 23 ± 2 decades μm^{-1}, independent of energy.

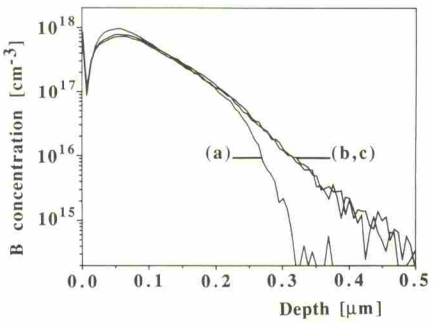

Fig. 2. Transient diffusion is illustrated for an implantation of 1×10^{13} cm^{-2}, 10 keV ^{11}B ions in Si(100) along [100]. The boron profiles are shown after implantation (a) and after anneals at 900 °C for 10 s (b) and 20 s (c). The results show that anomalous tail diffusion stops within 10 s at 900 °C.

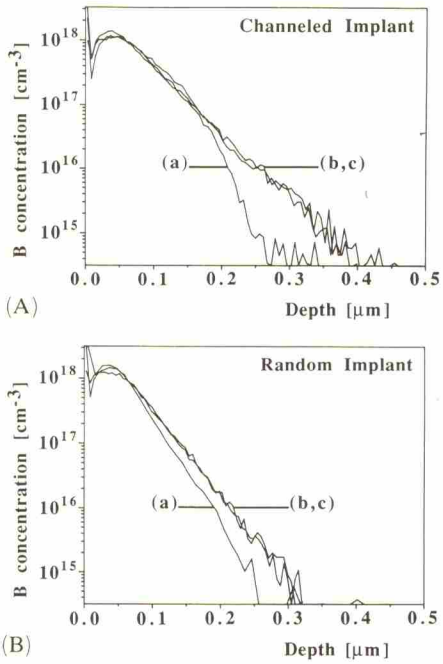

Fig. 3. SIMS profiles of 5 keV ^{11}B ions implanted to a dose of 1×10^{13} cm^{-2} in Si(100) along [100] (A) and random (B) directions. The boron profiles were measured after implantation (a) and after anneals for 10 s at 900 °C (b) and 1100 °C (c). The results illustrate the anomalous tail diffusion after high-temperature anneals for both implant conditions.

keV ^{11}B ions with RTA for 10 s at 950 °C. No residual defects are observed for the channeled implant (Fig. 4(A)), but for the implant in the random direction small dislocation loops ($\phi \approx 10$–20 nm) are present (Fig. 4(B)).

The anomalous boron tail diffusion for low-dose implants is a transient phenomenon, *i.e.* for boron implants of approximately 10^{13} cm^{-2} the anomalous diffusion stops within 10 s at 900 °C. However, for higher dose implants a different time dependence of boron diffusion is observed. In Fig. 5 SIMS profiles are shown for channeled implants of 2×10^{14} cm^{-2}, 380 keV ^{11}B ions (note that for this implant the boron peak concentration $C_p < n_i \approx 6\times10^{18}$ cm^{-3} at 900 °C, and thus concentration-enhanced diffusion is negligible). The as-implanted profile demonstrates the steep decay of the boron concentration at the substrate side, approximately 25 decades μm^{-1}. The change in the boron profile tail after RTA for 10 s at 900 °C, compared with the as-implanted profile, is too small to determine accurately the boron displacement. The diffusion after 15 min is significant and may be caused by evaporation of extended defects as will be discussed later.

The diffusion behavior for high-dose implants of boron ($C_p \gg n_i$) during RTA is illustrated in Fig. 6. SIMS profiles are shown for 5×10^{15} cm^{-2}, 100 keV

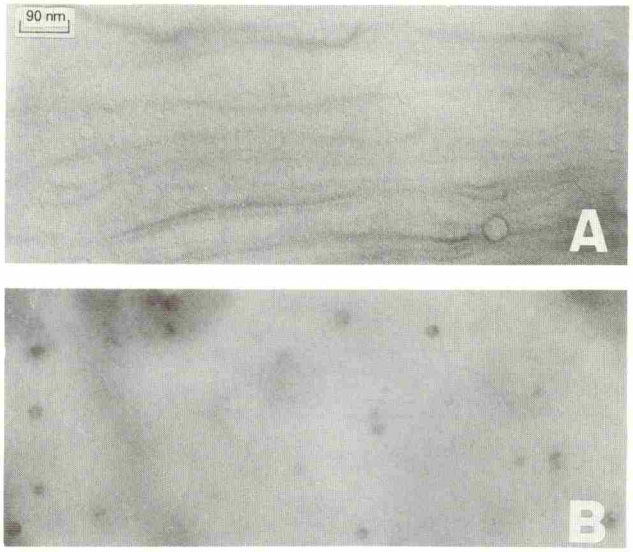

Fig. 4. Plan-view transmission electron micrographs after annealing for 10 s at 950 °C of Si(100) implanted with 1×10^{13} cm^{-2}, 5 keV ^{11}B ions in [100] (A) and random (B) directions. The sample which was implanted in a random direction contains small ($\phi \leq 20$ nm) dislocation loops. The channeling implant results in defect-free silicon.

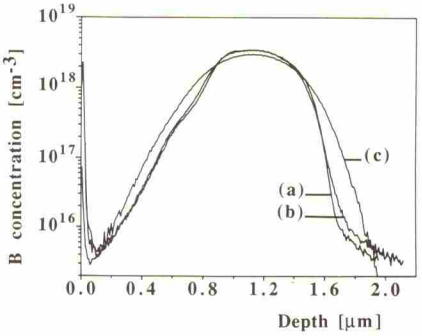

Fig. 5. Anomalous boron tail diffusion is illustrated for implants of 380 keV ^{11}B ions implanted to a dose of 2×10^{14} cm^{-2} in Si(100) along [100]. The boron profiles are shown after implantation (a) and after anneals at 900 °C for 10 s (b) and 15 min (c). Contrary to the results of low-dose implants, anomalous diffusion persists for longer times as shown by the result after annealing for 15 min.

^{11}B implants in [100] channeling and random directions. The as-implanted profile for the implant in a random direction peaks at a depth of 330 nm, in good agreement with the calculated projected range of 320 nm from transport and ranges of ions in matter (TRIM86) [58]. The channeling implant peaks at a depth of 440 nm. After RTA for 20 s at 900 °C transient boron tail diffusion is observed for both implant conditions. At a boron concentration of 2×10^{17} cm^{-3} the boron displacement is 58 nm for the channeling implant and 35 nm for the random implant. For both implants a kink in the tail of the boron profile results at a concentration of approximately 7×10^{18} cm^{-3}

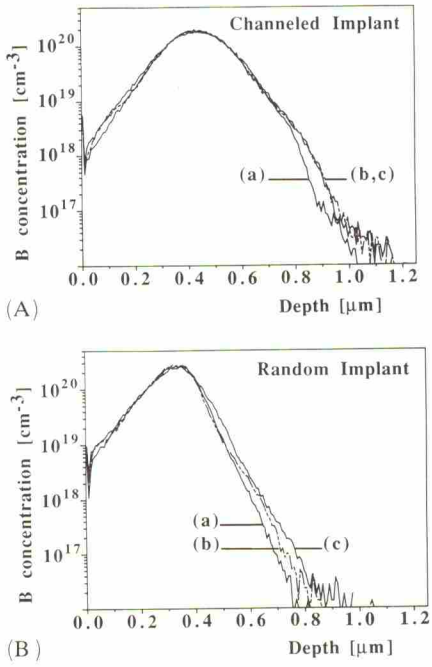

Fig. 6. Anomalous boron tail diffusion is illustrated for high-dose boron implants in Si(100). The implants were performed at an energy of 100 keV to a dose of 5×10^{15} cm^{-2} in [100] (A) and random (B) directions. SIMS profiles are shown after implantation (a) and after anneals for 20 s at 900 °C (b) and 1000 °C (c).

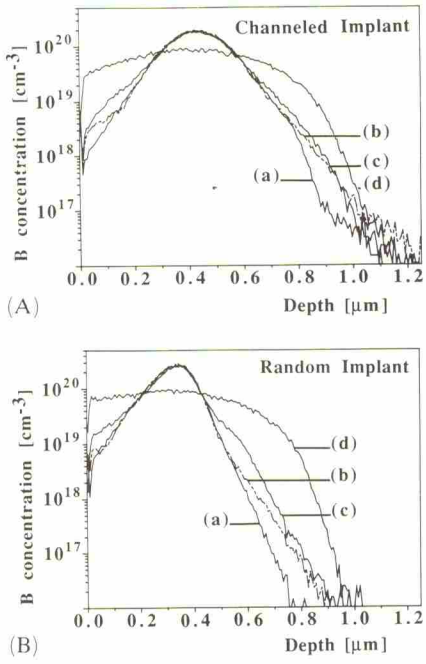

Fig. 7. Anomalous diffusion effects illustrated for boron implants in Si(100) after high-temperature furnace annealing. The implants were performed at an energy of 100 keV to a dose of 5×10^{15} cm^{-2} in [100] (A) and random (B) directions. SIMS boron profiles are shown after anneals for 30 min at 800 °C (b), 900 °C (c) and 1000 °C (d). The as-implanted boron profiles are also shown (a).

($n_i = 6\times10^{18}$ cm^{-3} at 900 °C). Above this concentration, referred to as C_{enh} [30, 59], no boron diffusion is observed for either implant conditions. After RTA for 20 s at 1000 °C no significant change in the boron profile compared with RTA for 20 s at 900 °C is observed for the implant in the [100] channeling direction below $C \approx 7\times10^{18}$ cm^{-3} (Fig. 6(a)). The transient boron tail diffusion below this concentration has apparently stopped. For the implant in a random direction anomalous diffusion is observed at 1000 °C in the tail region for concentrations above C_{enh}. A kink in the boron profile is seen at a concentration of approximately 10^{20} cm^{-3}, close to the solubility limit of $(1\text{–}1.1)\times10^{20}$ cm^{-3} at 1000 °C [60]. The boron profile above a concentration of 10^{20} cm^{-3} remains identical to the as-implanted profile for both implant conditions.

The effect of a longer annealing time on the (anomalous) boron diffusion in silicon for the high-dose implants is shown in Fig. 7 after anneals in a vacuum furnace for 30 min at 800, 900 and 1000 °C. Anomalous diffusion is observed for both implant conditions after annealing at 800 °C (b) if compared with the as-implanted profile (a). The profiles have a kink at a boron concentration of $C_{enh} \approx 3.5\times10^{18}$ cm^{-3} ($n_i = 3\times10^{18}$ cm^{-3} at 800 °C). Below C_{enh} anomalous boron diffusion is observed, while above C_{enh} no significant boron diffusion takes place. The boron displacement at a concentration of 2×10^{17} cm^{-3} is approximately 100 nm for the channeling implant and approximately 75 nm for the random implant and thus much larger than the intrinsic diffusion length ($L_{intr} \approx 2$ nm) [56]. After anneals for 30 min at 900 °C anomalous diffusion is observed at both the surface and substrate sides of the profiles (Fig. 7(c)) up to a concentration of $C_s \approx 6\times10^{19}$ cm^{-3} (C_s represents the solid solubility of boron in silicon at 900 °C). These results are consistent with those of Kim *et al.* [61] who showed that the static boron peak starts to become mobile at the end of the diffusion transient and concentration-enhanced diffusion starts. This effect has also been studied by means of electrical characterization. Integral Hall measurements were performed at room temperature. The results of the electrical measurements indicate that, for times in the range 20–60 s, the electrically active boron fraction remains constant and equal to 0.26 and 0.29 for the random and channeling implants respectively. After annealing for 120 s the electrically active fraction is 0.4 for both implant conditions, consistent with the results of Kim *et al.* [61]. SIMS profiles after anneals for 30 min at 1000 °C are also shown (Fig. 7(d)). Although the intrinsic diffusion length is substantial at 1000 °C ($L_{intr} \approx 50$ nm) [56], the actual diffusion is much larger for both implant conditions. The anomalous diffusion

is known as concentration-enhanced diffusion ($C_p > C_s$). The maximum boron concentration in the boron profiles after annealing is approximately 10^{20} cm^{-3}, equal to the solid solubility of boron in silicon at 1000 °C. Integral Hall measurements showed that in this case complete electrical activation of boron was achieved.

In this section we have illustrated that transient boron tail diffusion results from high-temperature anneals for short times (approximately 10–20 s). The transient boron tail diffusion behavior is similar for doses between 10^{13} and 5×10^{15} cm^{-2}. Furthermore, the present results show that anomalous boron diffusion persists for high boron doses if longer annealing times are applied at high temperatures. In the next section we illustrate the defect evolution for high-dose boron implants in silicon as a function of time at high temperatures and show that the anomalous boron diffusion encountered during longer annealing times is accompanied by evaporation of extended defects.

3.2. *Formation of extended defects*

In recent work we have shown that secondary defects form during high-temperature treatment in boron-implanted silicon if the total number of displaced silicon atoms exceeds a critical value of approximately 1.5×10^{16} cm^{-2} [62]. The high-dose implants (greater than 1×10^{14} cm^{-2}) considered in the previous section all give rise to a total number of displaced silicon atoms which exceeds the critical value. Therefore secondary defect formation is expected to occur simultaneously with the transient boron tail diffusion during high-temperature treatment. Secondary defects may influence boron transient diffusion and, in this section, the formation of extended defects and their effects on diffusion are discussed for the implants of 5×10^{15} cm^{-2}, 100 keV boron ions in silicon. These implants result in a total number of displaced silicon atoms of $N_{displ} \approx 1 \times 10^{17}$ cm^{-2} which is significantly above the critical value. (For high-dose (greater than 2×10^{15} cm^{-2}) implants of 100–200 keV boron ions in silicon at room temperature the total number of displaced silicon atoms is independent of implant condition. This is due to the dechanneling from the build-up of disorder as the dose is increased.)

Rutherford backscattering spectra in the [100] channeling direction are shown in Fig. 8 for samples implanted along [100] and in a random direction after anneals for 20 s at 800 °C (a), 900 °C (b) and 1000 °C (c). Also shown is a reference spectrum of unimplanted silicon (d). The amount of dechanneling increases very rapidly in the annealed samples in the regions between 300 and 480 nm below the silicon surface for the implants in the [100] direction, and between 190 and 345 nm for the implants in a random direction. A

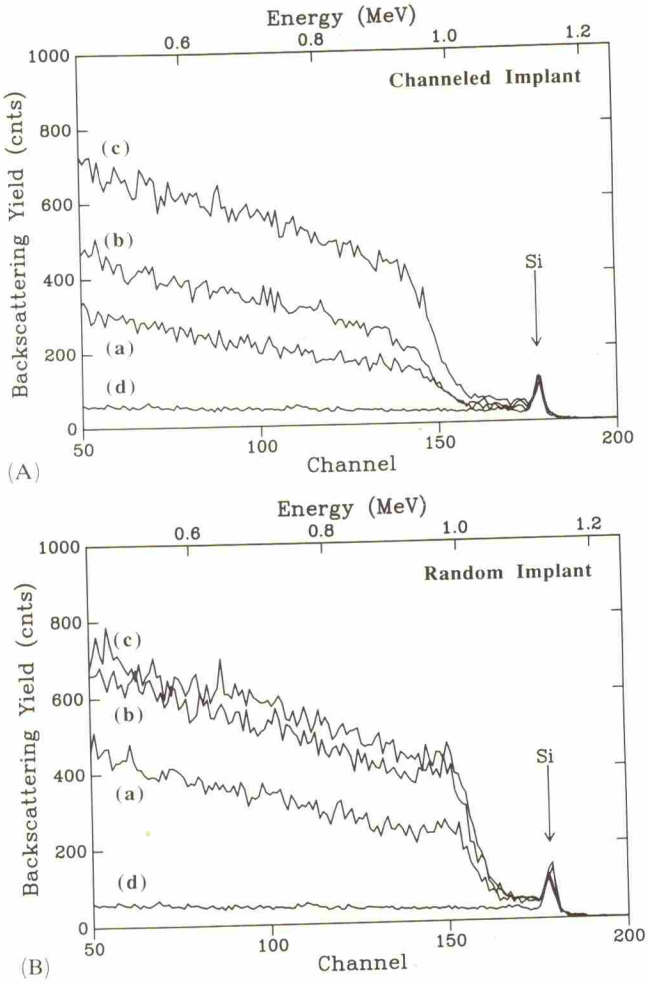

Fig. 8. Rutherford backscattering spectra in a channeling configuration for Si(100) samples implanted with 100 keV boron ions to a dose of 5×10^{15} cm^{-2} in [100] (A) and random (B) directions. The measurements were taken after anneals for 20 s at 800 °C (a), 900 °C (b) and 1000 °C (c). A channeling spectrum of unimplanted silicon is also shown (d). The channeling measurements illustrate the formation of extended defects during high-temperature annealing.

strong increase in the amount of dechanneling occurs in the regions which coincide with the peak positions of the damage distributions in the as-implanted silicon. Furthermore, the amount of dechanneling increases with temperature. The results are very similar for the random and channeling implants and indicate that extended defects are formed during annealing.

The effect of a longer annealing time on the dissolution of implantation damage is illustrated in Fig. 9 by RBS analysis in a channeling configuration. The results are shown for high-dose implants in a random direction after anneals for 30 min at 800 °C (a), 900 °C (b) and 1000 °C (c). Also shown is a reference spectrum of unimplanted silicon (d). After anneals at 800 and 900 °C channeling spectra are obtained which are very similar in shape to the spectra shown in Fig. 8 and

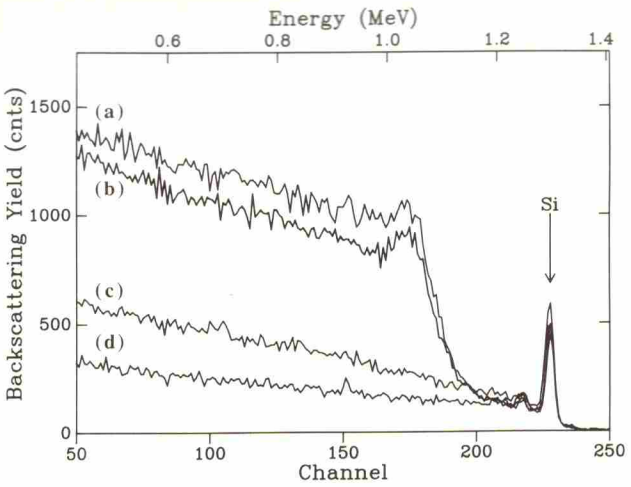

Fig. 9. Rutherford backscattering spectra in a channeling configuration for Si(100) samples implanted with 100 keV boron ions to a dose of 5×10^{15} cm^{-2} in a random direction after anneals for 30 min at 800 °C (a), 900 °C (b) and 1000 °C (c). A channeling spectrum of unimplanted silicon is also shown (d).

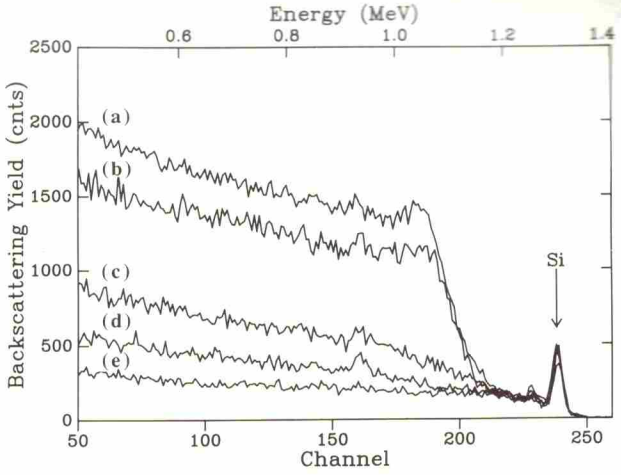

Fig. 10. The time evolution of extended defects is illustrated in Si(100) for random implants of 100 keV boron ions to a dose of 5×10^{15} cm^{-2}. Rutherford backscattering channeling spectra are shown after anneals at 1000 °C for 1 (a), 2 (b), 4 (c) and 8 min (d). A channeling spectrum of unimplanted silicon is also shown (e).

illustrate that a high concentration of extended defects must be present in the region 190–345 nm below the silicon surface. The profile obtained after annealing at 1000 °C shows a dramatic decrease in the amount of dechanneling, indicative of annealing of the extended defects. However, the increase in the amount of dechanneling with depth starting from the surface region is still considerably higher than for unimplanted silicon which indicates that some defects remain. The time evolution of the extended defects during annealing at 1000 °C has been more extensively investigated. Figure 10 shows the Rutherford backscattering spectra taken in the [100] direction after anneals for 1 min (a), 2 min (b), 4 min (c) and 8 min (d). The amount of dechanneling between channels 200 and 175 starts to decrease after a time of 1 min. For annealing times longer than 8 min the amount of dechanneling remains essentially unchanged. The channeling spectrum of unimplanted silicon is shown as a reference (e).

These samples have also been investigated by XTEM analysis to determine the character of the residual defects. Figure 11 shows cross-sectional transmission electron micrographs of the samples after anneals for 30 min at 800 °C (a) and 1000 °C (b). No residual defects are seen to a depth of 200 nm below the surface after annealing at 800 °C. From a depth of 200 to 350 nm a continuous band of dislocations is observed. Below this band of dislocations there is a low concentration of rod-shaped defects elongated along ⟨110⟩. The band of secondary defects results in the steep rise in the amount of dechanneling and the direct scattering peak which are observed in the channeling spectrum of Fig. 9 between channels 200 and 175. In

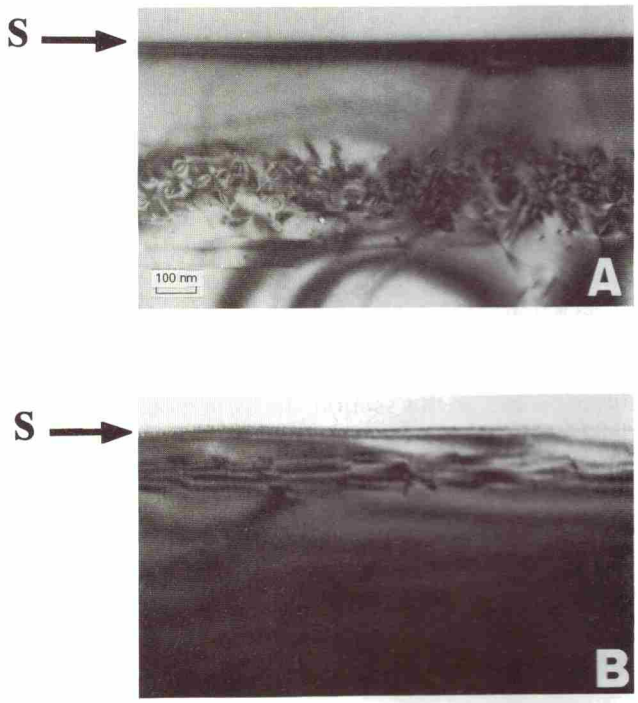

Fig. 11. Cross-sectional transmission electron micrographs of Si(100) implanted with 100 keV boron ions to a dose of 5×10^{15} cm^{-2} in a random direction. The micrographs were taken after anneals for 30 min at 800 °C (A) and 1000 °C (B). At a temperature of 1000 °C the extended defects which are positioned near the depth of the boron damage peak anneal out.

Fig. 11(B) a cross-sectional transmission electron micrograph is shown after annealing for 30 min at 1000 °C. The band of dislocations centered at a depth of 275 nm, observed in Fig. 11(A), has disappeared. A

low concentration of dislocations remains near this depth, corresponding to the position where the damage distribution is peaked in the as-implanted sample. Near a depth of 100 nm below the surface stacking faults are observed which cause the enhancement in the amount of dechanneling after an anneal of 30 min at 1000 °C (Fig. 9). The formation of such stacking faults after high-temperature annealing in high-dose, boron-implanted silicon has been observed previously for 40 and 70 keV boron ions [29, 63].

The present results show that high-temperature annealing of silicon implanted with a high dose of boron consists of two stages: in the first stage secondary defects form from condensation of point defects (see Fig. 8); if, however, the annealing temperature is high enough, prolonged annealing results in subsequent dissolution of the extended defects (see Fig. 10). In the previous section, we observed that anomalous boron tail diffusion is similar for low- and high-dose boron implants during short (10–20 s) anneals at high temperatures. However, we also found that longer annealing times (approximately 30 min) at 1000 °C result in anomalous boron diffusion for high-dose implants. From these results we can conclude that the evaporation of extended defects leads to further boron diffusion.

In the next section experimental results are provided which further illustrate the role of point defects and the formation and evaporation of extended defects on boron diffusion. The formation of point defects and extended defects is tailored by silicon implants to vary these conditions.

3.3. *Megaelectronvolt Si^+ irradiation*

Various studies on boron diffusion in silicon have illustrated that the diffusion behavior of boron can be influenced by additional irradiation with silicon ions prior to annealing [48, 49]. The silicon implants result in a supersaturation of point defects and, if the dose is sufficiently high, in extended defect formation. In this section the effect of introducing defects by megaelectronvolt silicon irradiation following low-energy boron implantation on the transient diffusion of boron atoms is investigated. Megaelectronvolt silicon irradiation was chosen because any extended defects caused by the 1 MeV silicon implants are formed well beyond the tail of the boron profile, while a nearly constant concentration of point defects is created within the boron profile. Wafers were implanted with 1×10^{13} cm^{-2}, 10 keV ^{11}B ions along the [100] channeling direction. Subsequent implants of 1 MeV ^{29}Si ions were performed at doses varying from 1×10^{10} to $5x10^{14}$ cm^{-2}. In Fig. 12 RBS measurements are shown in the [100] channeling direction for samples post-irradiated with 1×10^{10} (a), 1×10^{12} (b), 5×10^{13} (c), 1.5×10^{14} (d) and 5×10^{14} cm^{-2} (e), 1 MeV ^{29}Si ions. The channeling spectrum for unimplanted silicon (f) is shown as a reference. The channeling spectra of samples implanted with doses of 1×10^{10} and 1×10^{12} cm^{-2} are indistinguishable from the channeling spectrum for unimplanted silicon. For the other spectra, up to a depth of approximately 0.5 μm below the surface, the fraction of displaced atoms slowly increases and remains below about 1% even for the highest dose. The damage distribution for 1 MeV silicon implants peaks at about 1 μm below the surface. The concentration of displaced silicon atoms at a depth of about 0.3 μm (*i.e.* near the boron profile tail) was estimated from the channeling spectra to be in the range 1×10^{20} to 3×10^{20} cm^{-3} for silicon doses in the range 5×10^{13} to 5×10^{14} cm^{-2}. This number of displaced atoms is more than four orders of magnitude higher than the boron concentration in the tail region. For the two lowest doses of 1 MeV ^{29}Si ions the concentration of displaced silicon atoms was estimated from TRIM86 [58]. According to the calculations the concentrations at a depth of 0.3 μm correspond to 1×10^{17} and 1×10^{19} cm^{-3} for silicon doses of 1×10^{10} and 1×10^{12} cm^{-2} respectively, still at least one order of magnitude higher than the boron concentration in the tail region.

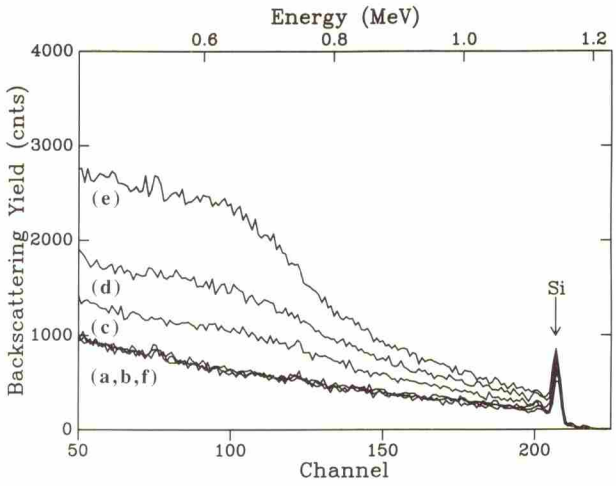

Fig. 12. RBS measurements in a channeling configuration of samples implanted with 1×10^{13} cm^{-2}, 10 keV ^{11}B ions along [100] and subsequently irradiated with 1.0 MeV ^{29}Si ions to doses of 10^{10} (a), 10^{12} (b), 5×10^{13} (c), 1.5×10^{14} (d) and 5×10^{14} cm^{-2} (e). Spectrum (f) is an unirradiated sample for reference.

From the channeling spectra the total number of displaced atoms was determined [64] to be 9×10^{16}, 2×10^{17} and 3.7×10^{17} cm^{-2} for the implants of 5×10^{13}, 1.5×10^{14} and 5×10^{14} cm^{-2} respectively. Details on the determination of the total number of displaced silicon atoms can be found in ref. 65. TRIM86 calculations were used to estimate the total number of displaced silicon atoms for the doses of 1×10^{10} and

1×10^{12} cm^{-2}, which resulted in 3×10^{13} and 3×10^{15} displaced silicon atoms cm^{-2} respectively. The TRIM86 value for the total number of displaced silicon atoms agrees reasonably well with the value estimated from RBS. The difference is within a factor of two for a dose of 5×10^{13} cm^{-2}, while for the highest dose the difference is a factor of four. The discrepancy between TRIM86 and RBS analysis may be due to dynamic annealing processes during implantation.

In Fig. 13 the SIMS boron profiles are shown after RTA for 10 s at 900 °C of samples irradiated with 1×10^{10}, 1×10^{12}, 5×10^{13}, 1.5×10^{14} and 5×10^{14} cm^{-2}, 1 MeV ^{29}Si ions, and for a sample which was not irradiated with 1 MeV silicon ions. The as-implanted boron profile is shown as a reference spectrum (a). The sample which was not irradiated with 1 MeV silicon ions shows that transient diffusion takes place during annealing in the tail of the boron profile (b). Identical diffusion behavior is observed in the tail of the boron profile for 1 MeV silicon irradiations of 1×10^{10} cm^{-2} (c) and 1×10^{12} cm^{-2} (d). In contrast, for a silicon dose of 5×10^{13} cm^{-2} or higher the transient diffusion is considerably reduced ((e)–(g)). Although the results in Fig. 13 show that after silicon irradiation at a sufficiently high dose the transient diffusion is reduced, it is still present. The diffusion length is considerably larger than expected for substitutional boron diffusion ($L_{intr} \approx 1$ nm at 900 °C for 10 s) [56]. It should also be noted that the reduction in boron transient tail diffusion is independent of silicon dose above 5×10^{13} cm^{-2}.

It is clear from the results shown in Fig. 13 that, in order to reduce transient diffusion, a threshold dose of 1 MeV silicon has to be exceeded. This critical dose lies in the range 10^{12} to 5×10^{13} cm^{-2}. XTEM was used to investigate the samples irradiated with doses of 1×10^{12} and 5×10^{13} cm^{-2}, 1.0 MeV ^{29}Si ions a annealed for 10 s at 900 °C (Fig. 14). No residu defects are observed in the sample irradiated with dose of 1×10^{12} cm^{-2}. In the sample irradiated w 5×10^{13} cm^{-2} ^{29}Si ions, no residual defects are prese within 0.5 μm of the surface, but from a depth of 0.5 1.0 μm an increasing concentration of dislocati loops is observed. Beyond a depth of 1.0 μm rc shaped defects along ⟨110⟩ directions are observ extending to a depth of 1.4 μm. At an energy of 1 M the critical number of displaced silicon atoms requir for secondary defect formation is generated for a dc of $(3–4) \times 10^{13}$ cm^{-2} [62]. During the anneal int stitials from the damaged region agglomerate at t peak position of the damage distribution and fo secondary defects. The results shown in Figs. 13 a 14 therefore suggest that the reduction in the transi

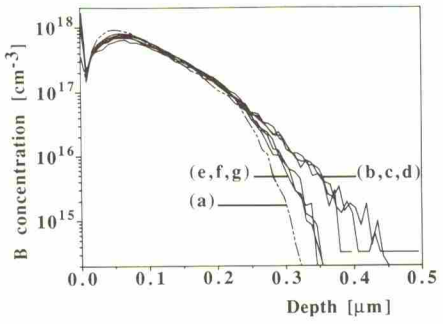

Fig. 13. SIMS profiles of boron after implantation of 1×10^{13} cm^{-2}, 10 keV ^{11}B ions along [100] (a); (b) similar to (a) after annealing for 10 s at 900 °C; (c), (d), similar to (a) after an additional irradiation with 10^{10} or 10^{12} cm^{-2}, 1.0 MeV ^{29}Si ions and subsequent annealing for 10 s at 900 °C; (e)–(g) similar to (a) after an additional irradiation of 1.0 MeV ^{29}Si ions to doses of 5×10^{13}, 1.5×10^{14} and 5×10^{14} cm^{-2} and subsequent annealing for 10 s at 900 °C.

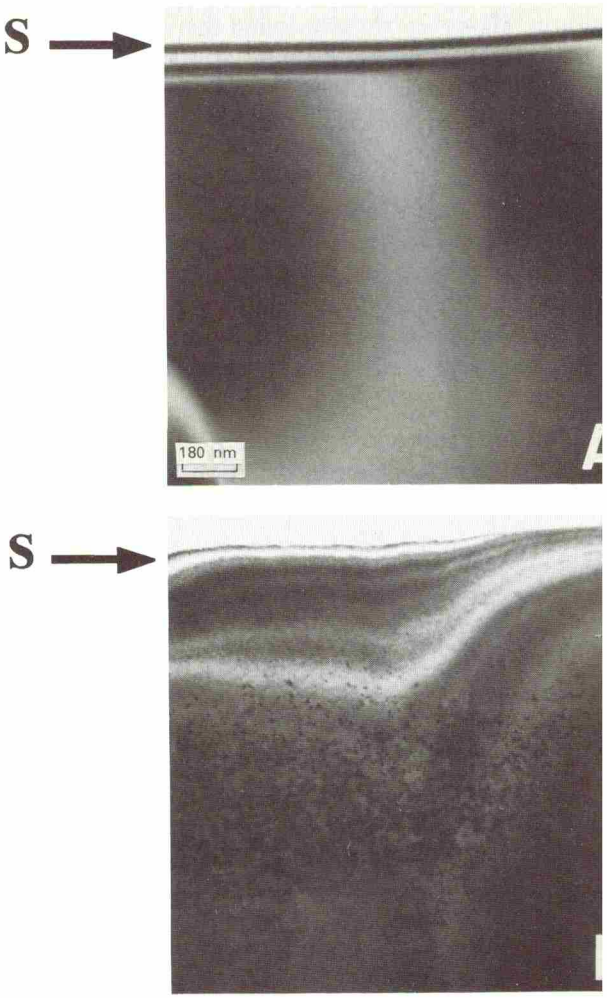

Fig. 14. Cross-sectional transmission electron micrograph Si(100) samples implanted with 10 keV ^{11}B ions to a dos 1×10^{13} cm^{-2} along [100] and subsequently implanted with MeV ^{29}Si ions to doses of 10^{12} (A) and 5×10^{13} cm^{-2} (B). micrographs were taken after annealing for 10 s at 900 °C.

diffusion is associated with the formation of extended defects.

After annealing for 10 s at 900 °C a reduction in the boron tail diffusion is observed if the irradiation dose of silicon ions is sufficiently high. The effect of annealing for a longer time is now discussed. In Fig. 15 SIMS profiles are shown for silicon samples implanted with 1×10^{13} cm^{-2}, 10 keV ^{11}B ions along the [100] channeling direction and subsequently irradiated with 1 MeV ^{29}Si ions to a dose of 1×10^{14} cm^{-2}. The silicon dose is sufficient to cause a reduction in the anomalous tail diffusion after annealing for 10 s at 900 °C (see also Fig. 13). The boron depth profiles are shown for the as-implanted sample (a) and after RTA at 900 °C for 10 s (b) and 2×10 s (c). In addition, the SIMS profile is presented for a sample which was not irradiated with 1.0 MeV ^{29}Si ions but annealed at 900 °C for 10 s (d). In agreement with the results of Fig. 13 a reduction in the transient boron tail diffusion is observed if the sample is irradiated with 1 MeV silicon and annealed for 10 s at 900 °C. However, after a subsequent anneal of 10 s the anomalous diffusion is observed again and is more pronounced for $10 \leqslant t \leqslant 20$ s than for $0 \leqslant t \leqslant 10$ s. The effect is ascribed to partial dissolution of secondary defects formed near a depth of 1 μm during the first annealing stage ($0 \leqslant t \leqslant 0$ s). This releases interstitials, enabling kick-out and thus fast boron diffusion.

The effect of prolonged annealing on the boron tail diffusion has been studied in more detail. The annealing of pre-existing secondary defects releases point defects and therefore may influence boron diffusion. Secondary defects were formed in silicon implanted with 1×10^{13} cm^{-2}, 10 keV boron ions by irradiation with 1 MeV ^{29}Si ions to doses of 2×10^{13}, 5×10^{13} and 5×10^{14} cm^{-2} followed by annealing for 10 s at 900 °C. XTEM analysis (not shown) confirmed that for all implants secondary defects are formed during RTA. A second anneal was performed in a vacuum furnace for 15 min at 1000 °C. Figure 16 shows the SIMS profiles for these samples. The as-implanted boron profile is shown as a reference (a). The boron depth profile is also shown for a sample irradiated with 5×10^{13} cm^{-2}, 1 MeV ^{29}Si ions and annealed for only 10 s at 900 °C (b). The sample irradiated with 5×10^{13} cm^{-2} ^{29}Si ions (d) shows the largest diffusion after 15 min at 1000 °C. Significantly less diffusion is observed for the sample irradiated with 2×10^{13} cm^{-2} ^{29}Si ions (c), while the sample implanted with the highest silicon dose (e) shows the least diffusion. Even for the sample with the highest silicon dose the boron tail diffusion is anomalous ($L_{intr} \approx 30$–45 nm at 1000 °C for 15 min) [56].

In Figs. 17(A) and 17(B) the cross-sectional transmission electron micrographs are shown for the samples after irradiation with 1 MeV ^{29}Si ions to a dose of 5×10^{13} cm^{-2}. Micrographs were taken after RTA for 10 s at 900 °C (A) and after subsequent annealing for 15 min at 1000 °C (B). Figure 17(A) is identical to Fig. 14(B) and shows the existence of a band of secondary defects between 0.5 and 1.0 μm below the silicon surface after annealing for 10 s at 900 °C. Figure 17(B) shows that, after subsequent annealing for 15 min at 1000 °C, the secondary defects have completely disappeared. At this high temperature extended defects release interstitials which enhance boron diffusion. Figure 18 shows Rutherford backscattering channeling spectra for the sample irradiated with 1.0 MeV ^{29}Si ions to a dose of 5×10^{14} cm^{-2} after annealing for 10 s at 900 °C (a). The spectra of unimplanted silicon in the [100] channeling direction (b) and a random direction (c) are also shown. The channeling spectrum of the implanted sample shows that the yield is nearly equal to that of unimplanted silicon down to channel 120.

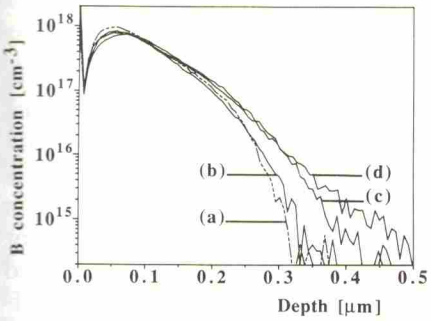

Fig. 15. SIMS profiles of 10 keV ^{11}B ions implanted to a dose of 1×10^{13} cm^{-2} along [100] in Si(100) after implantation (a); (b) similar to (a) after an additional implant of 1.0 MeV ^{29}Si ions to a dose of 1×10^{14} cm^{-2} and annealed for 10 s at 900 °C; (c) similar to (b) after subsequent annealing for 10 s at 900 °C. A SIMS profile of an unirradiated sample after annealing for 10 s at 900 °C (d) is shown as a reference.

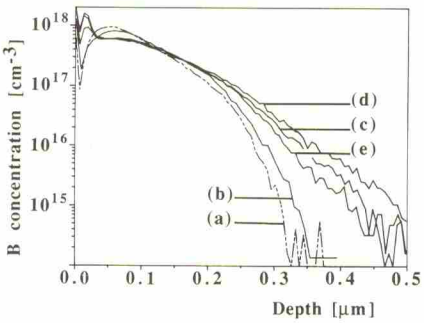

Fig. 16. SIMS profiles of 10 keV ^{11}B ions implanted to a dose of 1×10^{13} cm^{-2} along [100] in Si(100) after implantation (a), after additional irradiation with 5×10^{13} cm^{-2}, 1.0 MeV ^{29}Si ions followed by annealing for 10 s at 900 °C (b) and after additional implants of 2×10^{13} (c), 5×10^{13} (d) and 5×10^{14} cm^{-2} (e) followed by annealing for 10 s at 900 °C, with subsequent annealing for 15 min at 1000 °C.

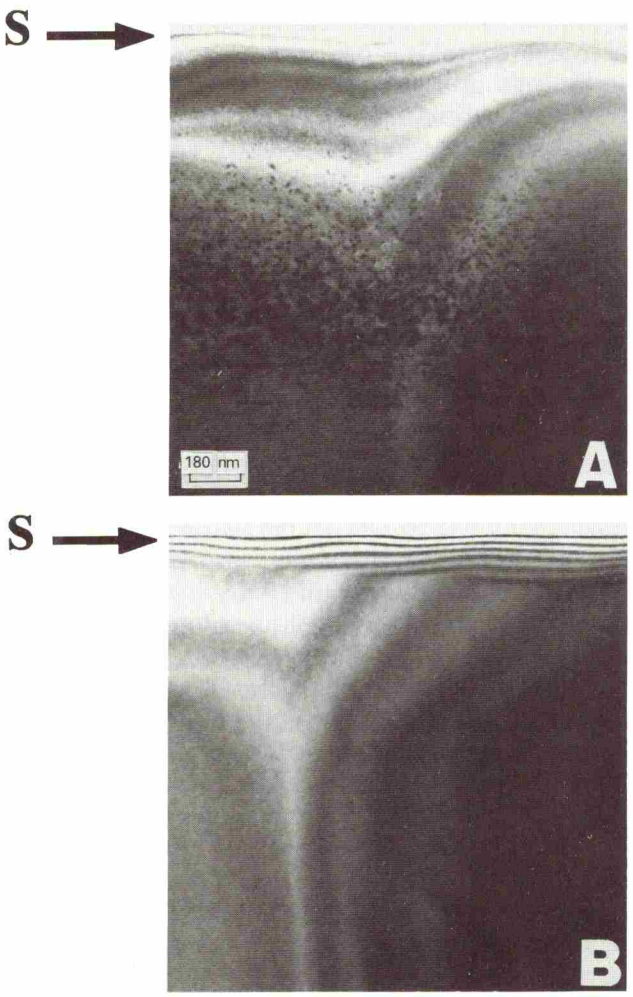

Fig. 17. Cross-sectional transmission electron micrographs of samples implanted with 10 keV ^{11}B ions to a dose of 1×10^{13} cm^{-2} along [100] and subsequently implanted with 1.0 MeV ^{29}Si ions to a dose of 5×10^{13} cm^{-2}. The micrographs were taken after annealing for 10 s at 900 °C (A) with subsequent annealing for 15 min at 1000 °C (B). The secondary defects present after annealing at 900 °C disappear during the second thermal treatment.

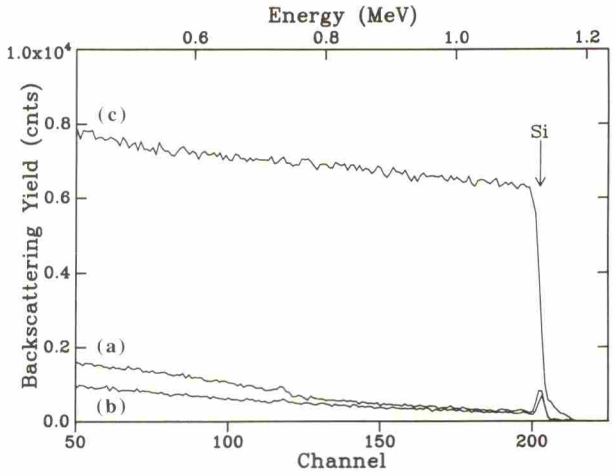

Fig. 18. RBS measurements in a channeling configuration of Si(100) implanted with 10 keV ^{11}B ions to a dose of 1×10^{13} cm^{-2} along [100] and subsequently with 5×10^{14} cm^{-2}, 1 MeV silicon ions and annealed for 10 s at 900 °C (a). The spectra of unimplanted silicon are also shown in the [100] channeling direction (b) and in a random direction (c).

Fig. 19. Cross-sectional transmission electron micrograph of a sample implanted with 10 keV ^{11}B ions to a dose of 1×10^{13} cm^{-2} along [100] and subsequently with 5×10^{14} cm^{-2}, 1 MeV silicon ions. The sample was annealed for 10 s at 900 °C followed by annealing for 15 min at 1000 °C. Extended defects ($\phi \approx 0.3$ μm) are observed at a depth of 1 μm below the surface.

Below this channel a strong increase in the amount of dechanneling is observed compared with that of unimplanted silicon, indicative of the presence of extended defects. In Fig. 19 a cross-sectional transmission electron micrograph is shown after additional annealing for 15 min at 1000 °C. Extended dislocations are observed (length, approximately 0.3 μm) near a depth of 1 μm below the surface. Therefore, in contrast with the sample irradiated with 10^{13} cm^{-2}, 1 MeV silicon ions, secondary defects remain. These results are consistent with the observations by Tamura and Natsuaki [66] who showed that, for high-dose megaelectronvolt implants (5×10^{14} cm^{-2} or greater), secondary defects can be annealed out only at temperatures of 1100 °C or higher.

In this section we have shown that transient boron tail diffusion can be significantly reduced if additional damage is introduced by means of megaelectronvolt silicon irradiation. The reduction of boron diffusion is associated with the formation of extended defects at larger depths. However, if the samples are annealed for longer times or at higher temperatures, extended defects evaporate and further anomalous boron diffusion is observed. This has been illustrated for silicon irradiations of 2×10^{13}, 5×10^{13} and 5×10^{14} cm^{-2}, 1 MeV silicon ions. Each implant results in secondary defect formation at a depth of 1 μm after annealing for 10 s at 900 °C. Further annealing for 15 min at 1000 °C results in (partial) evaporation of extended

defects and in anomalous boron tail diffusion. The effect is most significant for irradiation with 5×10^{13} cm^{-2}, 1 MeV silicon ions. XTEM illustrates that complete annealing of secondary defects is accomplished at 1000 °C. This also holds for irradiation with 2×10^{13} cm^{-2}, 1 MeV silicon ions but the number of evaporated secondary defects is much smaller. The highest silicon dose, *i.e.* 5×10^{14} cm^{-2}, results in the lowest diffusion rate. XTEM shows that extended defects remain after annealing and thus fewer interstitials are released. Apparently, the extent of anomalous diffusion depends on the number of extended defects which anneal out.

3.4. *Amorphization with ^{29}Si or ^{73}Ge ions*

The effect of post-amorphization on the boron tail diffusion was studied for silicon samples implanted with 1×10^{13} cm^{-2}, 10 keV ^{11}B ions along the [100] channeling direction. The samples were then amorphized with ^{28}Si or ^{73}Ge ions. The post-amorphization with silicon ions was accomplished by multiple implants of 5×10^{14} cm^{-2} at 125 keV, 1×10^{15} cm^{-2} at 200 keV and, finally, 1×10^{15} cm^{-2} at 400 keV. During the implants the samples were held at a temperature of −100 °C. Post-amorphization with germanium ions was accomplished by implants of 2×10^{14} cm^{-2} at 200 and 550 keV. During the germanium implants the samples were held at a temperature of −60 °C. These sets of implants amorphized surface layers of approximately 0.5 μm. The silicon parts of the channeling spectra are shown in Fig. 20 after post-amorphization with germanium ions (a), after recrystallization at 550 °C for 5 h (b) and after subsequent RTA at 900 °C for 10 s (c). The spectra of unimplanted silicon are shown for [100] channeling (d) and random (e) directions as reference. Annealing for 5 h at 550 °C ensures complete solid phase epitaxy (SPE) of the amorphized surface layer [67, 68]. The spectra taken after recrystallization and subsequent high-temperature annealing cannot be distinguished from that of unimplanted c-Si. RBS and channeling analysis of the germanium part of the spectra for samples implanted with germanium show that more than 90% of the germanium atoms are on substitutional sites after both SPE and subsequent RTA treatments, indicative of high-quality crystalline material.

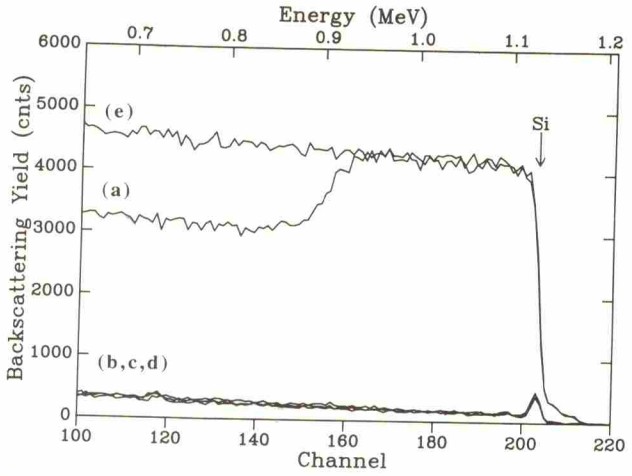

Fig. 20. RBS measurements in a channeling configuration of Si(100) implanted with 10 keV ^{11}B ions to a dose of 1×10^{13} cm^{-2} along [100] and subsequently with 2×10^{14} cm^{-2} ^{73}Ge ions at energies of 200 and 550 keV after implantation (a), annealing for 5 h at 550 °C (b) and annealing for 5 h at 550 °C followed by annealing for 10 s at 900 °C (c). The germanium implants were performed at −60 °C and result in an amorphized surface layer of 0.5 μm. After both anneals the channeling spectra are indistinguishable from unimplanted silicon. Spectra of unimplanted silicon in channeling (d) and random (e) directions are also shown.

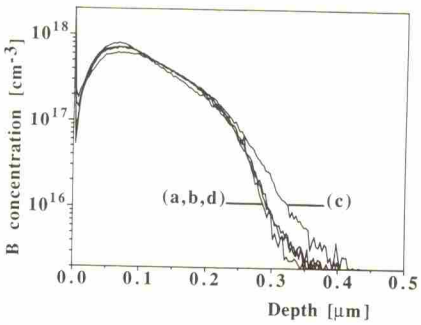

Fig. 21. SIMS profiles of silicon samples implanted with 10 keV ^{11}B ions to a dose of 1×10^{13} cm^{-2} along [100] after implantation (a), silicon post-amorphization and annealing for 10 s at 900 °C (b) and silicon post-amorphization and annealing for 5 h at 550 °C followed by annealing for 10 s at 900 °C (d). The SIMS profile for a sample which was not post-amorphized but annealed for 10 s at 900 °C (c) is shown as a reference.

The effect of post-amorphization with silicon or germanium ions on the boron depth profile is illustrated in Figs. 21 and 22 respectively. SIMS profiles are shown for an as-implanted sample (a) and for samples post-amorphized with silicon (Fig. 21) or germanium (Fig. 22) ions and annealed at 550 °C for 5 h followed by 900 °C for 10 s (b). The SIMS profiles for samples which were not amorphized but were given an identical thermal treatment are also shown (c). In Fig. 21 the boron depth profile is also shown for a sample which was post-amorphized and only annealed for 10 s at 900 °C (d). The samples which were not amorphized show transient boron tail diffusion. The post-amorphized samples do not show significant diffusion. Thus the post-amorphization procedure avoids transient boron tail diffusion.

In this section we have shown that boron transient tail diffusion can be avoided by amorphization of the surface layer of silicon such that the boron profile is completely incorporated in the amorphized layer.

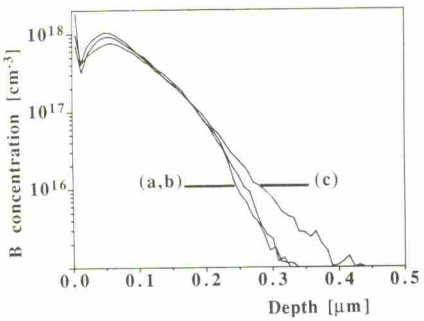

Fig. 22. SIMS profiles of silicon samples implanted with 10 keV ^{11}B ions to a dose of 1×10^{13} cm^{-2} along [100] after implantation (a), after additional germanium post-amorphization followed by annealing for 5 h at 550 °C and 10 s at 900 °C (b) and for a sample which was not post-amorphized but annealed for 10 s at 900 °C (c).

4. Discussion

In this section we show that our results are consistent with the idea that the phenomenon of transient diffusion of implanted boron in silicon is due to the kick-out mechanism. The interaction of interstitial silicon with boron atoms on lattice sites leads to the kick-out of boron atoms and thus the boron diffusivity is enhanced whenever interstitial silicon atoms are available. The influence of the formation of extended defects (stage I) and the annealing of extended defects (stage II) on boron diffusion is discussed. During stage I the concentration of mobile interstitials which are available for kick-out of substitutional boron atoms decreases with annealing time, whereas during stage II interstitials are released from the extended defects and boron diffusion is again enhanced.

4.1. Boron implants in silicon with $N < N_c$

In this section we discuss the boron diffusion behavior for every boron implant at a dose of 10^{14} cm^{-2} or less. These implants result in a total number of displaced silicon atoms below the critical number N_c of approximately 1.5×10^{16} cm^{-2} for secondary defect formation during annealing for 15 min at 900 °C [62]. Therefore the influence of extended defect formation and annihilation on (anomalous) boron diffusion can be neglected. Concentration-enhanced diffusion is also negligible because $C_p \ll n_i$. The results shown in Figs. 2 and 3 indicate that, for low-dose boron implants, the anomalous diffusion stops within 10 s at 900 °C, and thus can be referred to as transient. Similar observations have been made by others. Kim *et al.* [44, 45] have shown that anomalous boron tail diffusion stops within 10 s at 1000 °C for an implant of 1×10^{14} cm^{-2}, 15 keV boron ions in silicon, and within 1 s at 900 °C for an implant of 5×10^{13} cm^{-2}, 50 keV boron ions according to Hodgson *et al.* [27]. In both cases the total number of displaced silicon atoms is below N_c and no extended defects form during high-temperature treatment. Similar diffusion behavior has also been observed for phosphorus ions in silicon by Oehrlein *et al.* [15, 16]. They found that anomalous phosphorus tail diffusion stops within 10 s at 950 °C for an implant of 1×10^{14} cm^{-2}, 50 keV phosphorus ions in silicon. According to the kick-out mechanism, anomalous boron diffusion persists as long as mobile interstitial silicon atoms are available [69]. During high-temperature annealing the number of mobile interstitial silicon atoms will rapidly decrease due to annihilation, predominantly with vacancies, and thus the anomalous diffusion will stop as soon as no more silicon interstitials are available. Therefore, the present results are in agreement with the kick-out model.

The comparison in Fig. 3 between random and channeling low-dose boron implants shows that the anomalous diffusion in the profile tail is more prominent for channeling implants than for random implants. A similar behavior was observed by Chu *et al.* [39] for 5 keV boron implants to a dose of 2×10^{14} cm^{-2} and they suggested that the difference in the transient boron diffusion behavior reflects the difference in the distributions of the displaced silicon atoms. The random implants result in displacement of silicon atoms throughout the whole boron profile, whereas the channeling implants only displace silicon atoms in the EOR region [70]. Moreover, the overall damage level is larger for random implants than for channeling implants. Therefore, the present results may indicate that more boron atoms diffuse anomalously for a random implant than for a channeled implant. However, we observe more transient tail diffusion for the channeling implants than for the random implants because most of the implant damage results in the EOR region.

At first glance the difference in transient boron tail diffusion between the two different implant conditions appears to be related to the difference in secondary defect formation. The plan-view micrographs in Fig. 4 illustrate that, for implants of 1×10^{13} cm^{-2}, 5 keV boron ions in a random direction, small dislocation loops ($\phi \approx 10$–20 nm) result after annealing for 10 s at 950 °C, whereas for the channeling implants no residual defects are observed. The small dislocation loops observed in the near-surface region for the random implants are thought to be interstitial-type defects [71, 72]. Yet, these defects are not as stable as the extended defects observed after implantation of boron above a dose of approximately 10^{14} cm^{-2} (see ref. 73). The number of interstitials involved in the formation of the secondary defects was estimated from plan-view TEM analysis to be approximately 10^{1} cm^{-2}, considerably lower than the total number of di

placed silicon atoms of approximately 5×10^{14} cm^{-2} estimated from TRIM86 [58]. Therefore, the number of interstitials involved in the formation of secondary defects is small compared with the total number of displaced silicon atoms and the formation of these secondary defects may not significantly affect the anomalous boron tail diffusion. This also directly follows from further plan-view TEM investigations which show that the secondary defects are no longer present after annealing above 1050 °C instead of 950 °C, whereas in Fig. 3(b) the SIMS profiles after annealing for 10 s at 900 °C and 1100 °C are identical; thus annealing out the secondary defects has no effect on boron tail diffusion.

4.2. *Boron implants in silicon with $N > N_c$*

In this section boron implants generating a total number of displaced silicon atoms higher than N_c are considered. For these implants prolonged annealing at high temperatures may result in the shrinkage and eventually complete annealing of extended defects by the release of interstitials (stage II). Although secondary defects form at the peak of the boron damage distribution for sufficiently high boron doses, and thus the number of mobile interstitial silicon atoms strongly decreases due to secondary defect formation, the transient boron tail diffusion is not affected during stage I. This is illustrated in Fig. 6 for an implant of 5×10^{15} cm^{-2}, 100 keV boron ions along [100]. The total number of silicon atoms displaced by the implant is approximately 1×10^{17} cm^{-2} and thus secondary defects form at high temperatures. Despite the formation of secondary defects transient boron tail diffusion is observed. The boron displacement at a concentration of 2×10^{17} cm^{-2} is 58 nm for the channeling implant and 35 nm for the random implant. These results are consistent with those obtained from other experiments [6, 36]. The results obtained by Sedgwick *et al.* [6] illustrate that, for implants of 20 keV boron ions to a dose of $(1-3) \times 10^{15}$ cm^{-2} in silicon, transient boron tail diffusion occurs at a temperature of 950–1000 °C and stops within 10 s. The boron displacement deduced from their measurements is approximately 40–50 nm, in reasonable agreement with our results. Similar results were also obtained by Cho *et al.* [36] for 50 keV boron ions implanted to a dose of 1×10^{15} cm^{-2} in silicon after anneals for 10 s at 1050 °C or 1150 °C.

The present results strongly suggest that the kick-out mechanism during stage I is not affected by extended defect formation at the peak of the boron damage distribution. Silicon interstitials from the tail region, before being trapped by the extended defects at the peak of the boron damage distribution, will have to diffuse through the boron tail region and thus affect the boron diffusion by kick-out. Once the interstitials are trapped by the extended defects or annihilated the anomalous boron diffusion stops.

During stage II (*i.e.* during prolonged annealing after the formation of secondary defects has been completed), the extended defects (partially) anneal out. The effect of annealing out extended defects on boron diffusion has been illustrated for a few cases. In Fig. 5 the anomalous boron diffusion during stage II is shown for an implant of 2×10^{14} cm^{-2}, 380 keV boron ions along [100]. The SIMS profile was measured after annealing for 15 min at 900 °C. The boron diffusion below a concentration of $(1-2) \times 10^{18}$ cm^{-3} is anomalous at both sides of the boron profile. The resulting profile differs considerably from that obtained after annealing for 10 s at 900 °C. The implant results in a total number of displaced silicon atoms N_{displ} of approximately $(3-4) \times 10^{16}$ cm^{-2}, significantly higher than the critical number [62].

The effect of annealing out extended defects on boron diffusion behavior is further illustrated in Fig. 7 for implants of 100 keV boron ions to a dose of 5×10^{15} cm^{-2}. A high concentration of secondary defects results from these implants after annealing for 30 min at 800 °C (see Fig. 11). Anomalous diffusion is observed at this temperature below a boron concentration of approximately 3.5×10^{18} cm^{-3} (see Fig. 7). The boron diffusion behavior is predominantly ascribed to partial annealing of the extended defects. Annealing at 900 °C instead of 800 °C leads to further anomalous diffusion. Finally, after annealing at a temperature of 1000 °C, concentration-enhanced diffusion results in a flat profile with $C \approx C_s$. This is accompanied by annealing of the high concentration of secondary defects (see Fig. 11(B)).

Numerous experimental results can be found in the literature on anomalous boron diffusion in silicon implanted with medium (approximately 10^{14} cm^{-2}) or high (10^{15} cm^{-2} or greater) boron doses. Most experiments are consistent with the idea that the anomalous boron diffusion process consists of two stages if secondary defects are formed. A study on the anomalous boron diffusion by Oehrlein *et al.* [16] for implants of 1×10^{14} cm^{-2}, 30 keV boron ions has shown that anomalous boron tail diffusion stops within 10 s at 950 °C. However, annealing for 10 s at 1150 °C results in considerably more boron displacement. Similar results for isothermal anneals were found by Seidel *et al.* [13] and Miyake and Aoyama [74]. These results support the idea that at higher temperatures or during longer annealing times secondary defects (partially) anneal out and result in a continuation of the anomalous boron diffusion process by the release of mobile silicon interstitials. Apparently, the number of interstitials released due to annealing of the secondary

defects is sufficient in these experiments to result in significant boron displacement. Experiments by Kim *et al.* [44, 45, 61] illustrate similar behavior for higher dose (5×10^{14} and 2×10^{15} cm^{-2}, 15 keV boron ions) implants. They have shown that the transient boron tail diffusion stops within 10 s at 1000 °C, but after annealing for 40 s further anomalous diffusion is seen. Their XTEM analysis has shown that the anomalous diffusion observed after 40 s is accompanied by partial annealing of extended defects present after annealing for 10 s. Similar results have been reported for higher dose boron implants (10^{15} cm^{-2} or greater) [6, 75].

During the formation of secondary defects, mobile interstitial silicon atoms are very rapidly trapped or annihilated. However, boron tail diffusion is not affected, as explained earlier. Prolonged annealing results in shrinkage and eventually complete annealing of the secondary defects, and thus mobile interstitial silicon atoms are released. These mobile interstitials, if sufficient in number, result in the continuation of anomalous boron diffusion behavior.

4.3. Megaelectronvolt silicon irradiation of boron-implanted silicon

In this section the effect of 1 MeV silicon irradiation on transient boron diffusion in silicon is discussed. Megaelectronvolt silicon irradiation leads to the creation of point defects throughout the whole boron profile, while extended defects form well beyond the boron profile if the silicon dose is sufficiently high. Figure 13 shows that, for implants of 1 MeV silicon ions to a dose of 5×10^{13} cm^{-2} or higher, the transient boron tail diffusion is reduced. The formation of secondary defects at a depth of 1 μm, well beyond the boron profile tail, results in a decrease in the concentration of mobile interstitials near the boron profile tail, thereby reducing kick-out by silicon interstitials and also the effective diffusion length of boron in the tail region. The effect of megaelectronvolt silicon irradiation is identical for doses ranging from 5×10^{13} to 5×10^{14} cm^{-2}.

We have observed that, for boron implants which lead to secondary defect formation at the boron damage peak, no effect on the transient diffusion is observed during extended defect formation (stage I). However, for samples irradiated with 1 MeV silicon ions we observed a reduction in the transient boron tail diffusion. If secondary defects nucleate at the boron damage peak, silicon interstitials from the tail region have to diffuse through the boron profile to be captured by the secondary defects and thus give rise to anomalous boron diffusion. However, if secondary defects nucleate, at a depth well beyond the boron profile, the interstitials from the tail region diffuse away from the boron profile and do not give rise to kick-out of substitutional boron when diffusing to greater depths. Apparently, the position in which secondary defects form during stage I determines whether or not anomalous boron tail diffusion is reduced.

Only a few experiments can be found in the literature in which additional low-dose silicon implants have been performed to investigate the influence on (anomalous) boron diffusion. Recent results by Packan and Plummer [49] have illustrated that implants of 10^{12}–10^{13} cm^{-2}, 180 keV silicon ions in addition to 7×10^{11} cm^{-2}, 160 keV boron ions give rise to anomalous boron tail diffusion. Before the silicon implants were carried out the boron-implanted samples were annealed to activate the dopants. At first glance the outcome of this experiment seems to contradict our results for samples irradiated with 10^{10}–10^{14} cm^{-2}, 1 MeV silicon ions. However, the main difference between these two experiments is in the relative position of the vacancy and interstitial distributions. In the experiment of Packan and Plummer the EOR region of the silicon implant is close to the boron tail region. This EOR region is rich in silicon interstitials which can lead to enhancement of boron tail diffusion. In our experiment a nearly constant damage level was created throughout the boron profile by the low-dose high-energy silicon implants. Therefore the change in the excess silicon interstitial concentration in the boron tail region, caused by a low-dose implant of 1 MeV silicon ions, is balanced by the increase in the excess of vacancies and no significant effect is observed on the anomalous boron tail diffusion.

During annealing of extended defects (stage I) mobile interstitial silicon atoms are generated. The effect of the release of silicon interstitials on the boron diffusion is illustrated for low-dose boron implants in Figs. 15 and 16. Longer annealing at 900 °C ($t = 20$ s) results in further enhanced tail diffusion of boron in silicon irradiated with 10^{14} cm^{-2}, 1 MeV silicon ions (see Fig. 15). In contrast, the results for a sample which was not irradiated with silicon ions, but simultaneously annealed, show that the anomalous diffusion stops within 10 s (see Fig. 2). Clearly, the anomalous boron tail diffusion which takes place in the irradiated sample during $10 \leqslant t \leqslant 20$ s cannot result from individual mobile silicon interstitials which have survived annealing at 900 °C during $0 \leqslant t \leqslant 10$ s. Moreover, XTEM analysis after annealing for 10 s at 900 °C shows that secondary defects are formed (see Fig. 14). Therefore anomalous diffusion seems to result from (partial) annealing of extended defects.

The effect of annealing extended defects has been further illustrated for samples annealed at 1000 °C for 15 min subsequent to thermal treatment at 900 °C for 10 s. Here, it has been shown that the boron-implanted sample irradiated with 5×10^{13} cm^{-2} silicon ions

exhibits the largest diffusion. The cross-sectional transmission electron micrographs in Fig. 17 show that the anomalous boron diffusion is accompanied by complete annealing of extended defects, and thus by the release of a large number of interstitials. The anomalous diffusion shown in Fig. 16 for the sample irradiated with 2×10^{13} cm^{-2} silicon ions is less pronounced than that in the sample irradiated with 5×10^{13} cm^{-2} silicon ions because the concentration of extended defects is less after annealing for 10 s at 900 °C and thus a smaller number of interstitials are released during the subsequent anneal at 1000 °C. The anomalous boron diffusion at 1000 °C is lowest for the sample irradiated with 5×10^{14} cm^{-2}, 1 MeV silicon ions. The extended defects formed during annealing for 10 s at 900 °C (stage I) convert into more complex secondary defects during annealing for 15 min at 1000 °C (stage II) (see Fig. 19). The stability at 1000 °C of these defects induced by high-dose megaelectronvolt implants has been shown previously by Tamura *et al.* [76] for annealing times up to 113 h. If extended defects are stable against annealing, no mobile interstitial silicon atoms are released and boron diffusion is not anomalous.

Recently, various experiments have illustrated the role of the introduction of extra silicon interstitials by silicon implantation on anomalous boron diffusion. Bao and coworkers [46, 47] implanted 1×10^{15} cm^{-2}, 80 keV silicon ions in addition to 1×10^{15} cm^{-2}, 60 keV boron ions and found that, during annealing at 1000 °C, anomalous boron tail diffusion persists. Their XTEM analysis showed that the anomalous boron diffusion is accompanied by gradual annealing of extended defects. They explained their data by assuming that the shrinkage of the extended defects and thus the release of mobile interstitial silicon atoms causes the anomalous boron tail diffusion. An implant of 1×10^{15} cm^{-2}, 60 keV boron ions alone leads to extended defect formation at high temperatures because a significantly larger number of silicon atoms are displaced than the critical number N_c needed to form secondary defects. Therefore the experiments by Bao and coworkers show the effect of annealing extended defects on boron diffusion behavior, irrespective of whether the extended defects result from the boron or silicon implant. The effect of an additional silicon implant more directly follows from the experiments by Packan and Plummer [49] and Michel *et al.* [48]. In the experiment by Packan and Plummer, 1×10^{14} cm^{-2}, 180 keV silicon ions were implanted in silicon which was first implanted with 7×10^{11} cm^{-2}, 160 keV boron ions and annealed for 10 min at 900 °C. They observed anomalous boron diffusion during subsequent high-temperature anneals. The implant of 1×10^{14} cm^{-2}, 180 keV silicon ions results in secondary defect formation. The anneal for 10 min at 900 °C results in partial annihilation of the secondary defects and thus in enhanced boron diffusion. A similar result was found by Michel *et al.* [48] who showed that significantly more boron tail diffusion is observed during an anneal for 35 min at 800 °C if, in addition to 2×10^{14} cm^{-2}, 60 keV boron ions, an implantation of 1×10^{14} cm^{-2}, 130 keV silicon ions is performed. Again, the silicon implant results in the formation of secondary defects at high temperatures, but during prolonged annealing secondary defects start to shrink in size and eventually anneal out, thereby resulting in enhanced boron tail diffusion. Servidori *et al.* [37, 70] have shown that anomalous boron tail diffusion is observed if boron-implanted samples are post-amorphized with silicon ions such that the boron profile tail is just beyond the amorphous–crystalline transition region (*i.e.* the boron profile tail is in the interstitial-rich region of the silicon implant). In this case interstitials in the transition region can either form EOR dislocation loops or result in kick-out of substitutional boron atoms.

4.4. *Post-amorphization implants with silicon or germanium ions*

In Figs. 21 and 22 the results of post-amorphization implants with silicon and germanium ions are given. After SPE regrowth and subsequent high-temperature RTA, boron profiles are obtained which are indistinguishable from the as-implanted profiles. During recrystallization of the amorphized surface layer, boron atoms are positioned on substitutional sites and no (clusters of) interstitials remain in the regrown layers. Therefore no anomalous boron diffusion takes place in the recrystallized layer by kick-out of substitutional boron during subsequent high-temperature annealing. The results show that post-amorphization is a useful technique to avoid anomalous boron diffusion and does not lead to the restriction of gaussian-shaped profiles as does pre-amorphization. The interstitials which are produced beyond the amorphous–crystalline transition in the crystalline substrate cannot give rise to anomalous boron tail diffusion because they are trapped by the EOR dislocation loops [6, 75]. It should be noted that, in the present experiments, the boron profiles were completely incorporated in the amorphized surface region. However, if the boron profile tail extends into the crystalline substrate, anomalous boron diffusion is observed as described in Sections 4.1 and 4.2.

5. Conclusions

Anomalous tail diffusion of low-dose (approximately 10^{13} cm^{-2}) implants of boron in c-Si is a

transient phenomenon. More anomalous tail diffusion is observed for channeling implants than for random implants because more boron atoms dechannel in the tail region, giving rise to a high concentration of interstitials there. The overall damage level is higher for random than for channeling implants and thus a larger number of interstitial silicon atoms result in the kick-out of boron atoms.

For higher dose boron implants (approximately 10^{14} to 5×10^{15} cm^{-2}), two stages are recognized in the boron diffusion process at high temperatures which are related to the evolution of extended defects. During the first stage extended defects are formed at the position in which the boron damage profile peaks. Although this reduces the concentration of mobile interstitials it does not influence the transient boron tail diffusion. Annealing of extended defects (stage II) results in the release of interstitials. This process results in further anomalous boron diffusion.

The effect of megaelectronvolt silicon irradiations on boron tail diffusion has been illustrated. Reduction of transient boron tail diffusion is observed for short annealing times, *i.e.* $t \approx 10$ s, if the silicon implant is performed at a sufficiently high dose to result in secondary defect formation at a depth of 1 μm (stage I). During prolonged annealing these extended defects anneal out (stage II) and give rise to anomalous boron diffusion behavior due to the generation of mobile interstitials.

Post-amorphization with silicon or germanium ions eliminates anomalous boron tail diffusion if the boron profile is completely incorporated in the amorphized region.

Acknowledgments

We wish to thank J. J. M. Ottenheim (Philips Research Laboratories, The Netherlands) for his help with electrical characterization. This work is part of the research program of the Stichting voor Fundamenteel Onderzoek der Materie (FOM) and was made possible by financial support from the Nederlandse Organisatie voor Wetenschappelijk Onderzoek (NWO) and Varian/Extrion (U.S.A.).

References

1 R. Kakoschke and K. Ehinger, *Nucl. Instrum. Methods B, 37/38* (1989) 823.
Y. Akasaka, *Nucl. Instrum. Methods B, 37/38* (1989) 9.
M. Tokuyama, *Nucl. Instrum. Methods B, 37/38* (1989) 744.
2 S. N. Hong, G. A. Ruggles, J. J. Wortman, E. R. Myers and J. J. Hren, *IEEE Trans. Electron Devices, 38* (1991) 28.
S. N. Hong, G. A. Ruggles, J. J. Wortman and M. C, Öztürk, *IEEE Trans. Electron Devices, 38* (1991) 476.
3 D. R. Myers and R. G. Wilson, *Radiat. Eff., 47* (1980) 91.
4 A. E. Michel, R. H. Kastl, S. R. Mader, B. J. Masters and J. A. Gardner, *Appl. Phys. Lett., 44* (1984) 404.
5 H. Ishiwara and S. Horita, *Jpn. J. Appl. Phys., 24* (1985) 568.
6 T. O. Sedgwick, A. E. Michel, V. R. Deline, S. A. Cohen and J. B. Lasky, *J. Appl. Phys., 63* (1988) 1452.
7 D. K. Sadana, E. Myers, J. Liu and T. Finstad, *Mater. Res. Soc. Symp. Proc., 23* (1984) 303.
8 M. C. Ozturk and J. J. Wortman, *Appl. Phys. Lett., 52* (1988) 281.
9 S. R. Wilson, W. M. Paulson, R. B. Gregory, B. C. Lamartine, J. A. Leavitt, L. C. McIntyre and J. L. Seerveld, *Nucl. Instrum. Methods B, 21* (1987) 433.
10 A. La Ferla, S. Cannavò, G. Ferla, V. Raineri and E. Rimini, in *Proc. 17th European Solid State Res. Conf., Bologna, 1987*, p. 429.
11 S.-J. Kwon, H.-J. Kim and J.-D. Lee, *Jpn. J. Appl. Phys., 29* (1990) L2326.
12 R. Bader and S. Kalbitzer, *Radiat. Eff., 6* (1970) 211.
13 T. E. Seidel, D. J. Linscher, C. S. Pai, R. V. Knoell, D. M. Maher and D. C. Jacobson, *Nucl. Instrum. Methods B, 7/8* (1985) 251.
14 R. B. Fair, in Z. Shichang (ed.), *Proc. Shanghai Workshop on Ion Implantation, Ion Beam Laboratory, Shanghai Institute of Metallurgy, Academia Sinica, Hangzhou, China, 1988*, p. 12; *Mater. Res. Soc. Symp. Proc., 35* (1985) 381.
15 G. S. Oehrlein, S. A. Cohen and T. O. Sedgwick, *Appl. Phys. Lett., 45* (1984) 417.
16 G. S. Oehrlein, R. Ghez, J. D. Fehribach, E. F. Gorey, T. O. Sedgwick, S. A. Cohen and V. R. Deline, in L. C. Kimerling and J. M. Parsey, Jr. (eds.), *Proc. 13th Int. Conf. on Defects in Semiconductors, Coronado, CA, August 12–17, 1984*, The Metallurgical Society and The American Institute of Materials Engineering, Warrendale, PA, 1984, p. 539.
17 N. E. B. Cowern, D. J. Godfrey and D. E. Sykes, *Appl. Phys. Lett., 49* (1986) 1711.
18 P. Negrini, M. Servidori and S. Solmi, *Philos. Mag. A, 61* (1990) 553.
19 F. F. Morehead and R. T. Hodgson, *Mater. Res. Soc. Symp. Proc., 35* (1985) 341.
20 J. Narayan, *J. Appl. Phys., 53* (1982) 8607.
21 K. S. Jones and D. Venables, *J. Appl. Phys., 69* (1991) 2931.
22 A. C. Ajmera and G. A. Rozgonyi, *Appl. Phys. Lett., 49* (1986) 1269.
A. C. Ajmera, G. A. Rozgonyi and R. B. Fair, *Appl. Phys. Lett., 52* (1988) 813.
23 R. J. Schreutelkamp, W. X. Lu, F. W. Saris, K. T. F. Janssen, J. J. M. Ottenheim, R. E. Kaim and J. F. M. Westendorp, *Mater. Res. Soc. Symp. Proc., 157* (1990) 691.
24 A. E. Michel, *Nucl. Instrum. Methods B, 37/38* (1989) 379.
25 W. Wach and K. Wittmaack, *Nucl. Instrum. Methods, 194* (1982) 113.
26 W. K. Hofker, H. W. Werner, D. P. Oosthoek and H. A. M. de Grefte, Appl. Phys., 2 (1973) 265; *Philips Res. Rep., Suppl., 8* (1975).
27 R. T. Hodgson, V. R. Deline, S. Mader, F. F. Morehead and J. C. Gelpey, *Mater. Res. Soc. Symp. Proc., 23* (1984) 253; *Appl. Phys. Lett., 44* (1984) 589.
28 L. C. Hopkins, T. E. Seidel, J. S. Williams and J. C. Bean, *J. Electrochem. Soc., 132* (1985) 2035.
29 W. K. Hofker, *PhD Thesis*, University of Amsterdam, 1975.
30 R. B. Fair, J. J. Wortman and J. Liu, *J. Electrochem. Soc., 131* (1984) 2387.
31 A. E. Michel, W. Rausch, P. A. Ronsheim and R. H. Kastl, *Appl. Phys. Lett., 50* (1987) 416.
32 B. J. Masters and E. F. Gorey, *J. Appl. Phys., 49* (1978) 2717.

33 T. Tsuchimoto and T. Tokuyama, *Radiat. Eff., 6* (1970) 121.
34 S. M. Hu, *J. Appl. Phys., 45* (1974) 1567.
35 P. Fahey, R. W. Dutton and M. Moslehi, *Appl. Phys. Lett., 43* (1983) 683.
P. Fahey, G. Barbuscia, M. Moslehi and R. W. Dutton, *Appl. Phys. Lett., 46* (1985) 784.
36 K. Cho, M. Numan, T. G. Finstad, W. K. Chu, J. Liu and J. J. Wortman, *Appl. Phys. Lett., 47* (1985) 1321.
37 M. Servidori, R. Angelucci, F. Cembali, P. Negrini, S. Solmi, P. Zaumseil and U. Winter, *J. Appl. Phys., 61* (1987) 1834.
38 H. Metzner, G. Sulzer, W. Seelinger, B. Ittermann, H.-P. Frank, B. Fischer, K.-H. Ergezinger, R. Dippel, E. Diehl, H.-J. Stöckmann and H. Ackermann, *Phys. Rev. B, 42* (1990) 11 419.
39 W.-K. Chu, M. Z. Numan, J. Z. Zhang, G. S. Sandhu and A. E. Michel, *Nucl. Instrum. Methods B, 37/38* (1989) 365.
40 R. Kalish, G. S. Oehrlein, V. R. Deline and S. A. Cohen, *Nucl. Instrum. Methods, B, 7/8* (1985) 329.
41 D. Fan, J. Huang, R. J. Jaccodine, P. Kahora and F. Stevie, *Appl. Phys. Lett., 50* (1987) 1745.
42 F. Cembali, M. Servidori, E. Landi and S. Solmi, *Phys. Status Solidi A, 94* (1986) 315.
43 G. D. Watkins, *Phys. Rev. B, 12* (1975) 5824.
44 Y. M. Kim, G. Q. Lo, D. L. Kwong, A. F. Tasch and S. Novak, *Appl. Phys. Lett., 56* (1990) 1254.
45 Y. M. Kim, G. Q. Lo, D. L. Kwong, H. H. Tseng and R. Hance, *Mater. Res. Soc. Symp. Proc., 146* (1989) 391.
46 X. Bao, Q. Guo, M. Hu and D. Feng, *J. Appl. Phys., 66* (1989) 1475.
47 Q. Guo, X. Bao, J. Hong, Y. Yan and D. Feng, *Appl. Phys. Lett., 54* (1989) 1433.
48 A. E. Michel, W. Rausch and P. A. Ronsheim, *Appl. Phys. Lett., 51* (1987) 487.
49 P. A. Packan and J. D. Plummer, *Appl. Phys. Lett., 56* (1990) 1787.
50 V. Raineri, R. J. Schreutelkamp, F. W. Saris, K. T. F. Janssen and R. E. Kaim, *Appl. Phys. Lett., 58* (1991) 922.
51 D. W. Berrian, R. E. Kaim, J. W. Vanderpot and J. F. M. Westendorp, *Nucl. Instrum. Methods B, 37/38* (1989) 500.
D. W. Berrian, R. E. Kaim and J. W. Vanderpot, *Nucl. Instrum. Methods B, 37/38* (1989) 518.
J. D. Pollock, R. W. Milgate, R. F. McRay and R. E. Kaim, *Nucl. Instrum. Methods B, 37/38* (1989) 576.
52 A. Polman, A. M. Vredenberg, W. H. Urbanus, P. J. van Deenen, H. Alberda, H. Krop, I. Attema, E. de Haas, H. Kersten, S. Doorn, J. Derks, J. ter Beek, S. Roorda, R. Schreutelkamp, J. G. Bannenberg and F. W. Saris, *Nucl. Instrum. Methods B, 37/38* (1989) 935.
53 E. V. Kornelsen, F. Brown, J. A. Davies, B. Domeij and G. R. Piercy, *Phys. Rev., 136* (1964) A849.
54 O. B. Firsov, *Sov. Phys. JETP, 36* (1959) 1076.
55 R. J. Schreutelkamp, F. W. Saris, R. E. Kaim, J. F. M. Westendorp and K. T. F. Janssen, unpublished work, 1989.
56 A. A. Brown, P. B. Moynagh and P. J. Rosser, in *Properties of Silicon*, Emis Datareviews Series No. 4, INSPEC, 1988, p. 327.
57 S. Matsumoto, Y. Ishikawa and T. Niimi, *J. Appl. Phys., 54* (1983) 5049.
58 J. P. Biersack and L. G. Haggmark, *Nucl. Instrum. Methods, 174* (1980) 257.
59 N. E. B. Cowern, K. T. F. Janssen and H. F. F. Jos, *J. Appl. Phys., 68* (1990) 6191.
60 D. Nobili, in *Properties of Silicon*, Emis Datareviews Series No. 4, INSPEC, 1988, p. 384.
61 Y. M. Kim, H. Z. Massoud and R. B. Fair, *J. Electron. Mater., 18* (1989) 143.
62 R. J. Schreutelkamp, J. R. Liefting, J. S. Custer, W. X. Lu, V. Raineri, F. W. Saris, K. T. F. Janssen, R. E. Kaim, P. H. F. M. van der Meulen and J. F. M. Westendorp, *7th Int. Conf. on Ion Beam Modification of Materials, Knoxville, TN, USA*, 1990.
R. J. Schreutelkamp, J. S. Custer, J. R. Liefting and F. W. Saris, *Appl. Phys. Lett., 58* (1991) 2827.
63 S. Mader, in J. F. Ziegler (ed.), *Ion Implantation: Science and Technology*, Academic Press, New York, 1984, p. 84.
64 W.-K. Chu, J. W. Mayer and M.-A. Nicolet (eds.), *Backscattering Spectrometry*, Academic Press, New York, 1978.
65 R. J. Schreutelkamp, J. S. Custer, J. R. Liefting, W. X. Lu and F. W. Saris, *Mater. Sci. Rep., 6* (1991) 275–366.
66 M. Tamura and N. Natsuaki, *Jpn. J. Appl. Phys., 25* (1986) L474.
67 L. Csepregi, E. F. Kennedy, T. J. Gallagher, J. W. Mayer and T. W. Sigmon, *J. Appl. Phys., 48* (1977) 4234.
68 G. L. Olson and J. A. Roth, *Mater. Sci. Rep., 3* (1988) 1–77.
69 S. Solmi, F. Baruffaldi and R. Canteri, *J. Appl. Phys., 69* (1991) 2135.
70 M. Servidori, Z. Sourek and S. Solmi, *J. Appl. Phys., 62* (1987) 1723.
71 R. S. Nelson, in *Proc. Int. Conf. on Radiation Damage and Defects in Semiconductors, Reading, U.K., 1972*, p. 140.
72 J. W. Corbett, J. P. Karins and T. Y. Tan, *Nucl. Instrum. Methods, 182/183* (1981) 457.
73 C. R. Peter, J. P. de Souza and C. M. Hazenack, *J. Appl. Phys., 64* (1988) 2696.
74 M. Miyake and S. Aoyama, *J. Appl. Phys., 63* (1988) 1754.
75 J. Narayan and O. W. Holland, *J. Appl. Phys., 56* (1984) 2913.
76 M. Tamura, N. Natsuaki, Y. Wada and E. Mitani, *J. Appl. Phys., 59* (1986) 3417.